FUDMA Journal of Engineering and Technology
ISSN: 3092-9385
https://fjet.fudutsinma.edu.ng/index.php/fjet/
Volume 2, Issue 1, 2026, 695-706

Influence of Process Variables on the Adsorption of Methylene Blue from Aqueous Solution Using Iron-Modified Zeolite A

Esther M. GANA[1*], Umaru MUSA[2], Abdulsalami S. KOVO[3]

[1*,2,3]Department of Chemical Engineering, Federal University Technology, Minna, Nigeria

[1*]esther.gana@futminna.edu.ng, [2]umar.musa@futminna.edu.ng, [3]kovo@futminna.edu.ng

Abstract

This study presents the synthesis and characterization of iron-modified zeolite-A derived from Nigerian kaolin for methylene blue adsorption. Zeolite-A was synthesized via hydrothermal alkaline activation of metakaolin, followed by iron functionalization using $FeCl_3 \cdot 6H_2O$. Materials were characterized by XRD, FTIR, SEM, XRF, and BET. XRD confirmed phase-pure zeolite-A with an LTA framework (peaks at 7.14°, 24.06° 2θ) and crystallite size of 20.74 nm. After iron incorporation, the framework remained intact while new iron-related reflections appeared at 44.8° and 65.20°, with crystallite size reducing to 9.06 nm. FTIR verified the aluminosilicate framework with peaks at 3724.94 and 3471–3466 cm^{-1} (Si-O-T vibrations), with additional Fe-O bands after modification. SEM showed typical cubic morphology preserved but with surface texturing after iron loading. BET of Fe-modified zeolite A gave a surface area of 380.350 $m^2 g^{-1}$ with Type IV isotherms (hierarchical micro-mesoporosity), versus 515.22 $m^2 g^{-1}$ for pristine zeolite A. XRF confirmed iron incorporation: Fe_2O_3 increased from 2.26 to 9.83 wt.%, and Si/Al ratio rose from 1.36 to 1.89 due to Na^+ exchange and partial dealumination. Batch adsorption of MB using the iron modified zeolite A under optimum dosage, initial concentration, contact time of 0.6 g, 6mg/L and 90 min resulted to 99.6% methylene blue removal, outperforming unmodified zeolite-A (98.3). The preserved zeolite A framework, enhanced adsorption potential, and hierarchical porosity positions the iron-modified zeolite-A as a promising adsorbent for MB removal from dye contaminated wastewater.

Keywords: *Adsorption, characterization, Fe-modification, Methylene Blue, Zeolite-A.*

1.0 Introduction

Globally, industrialization and modernization of cities has appreciably increased the water demand and utilization, thus resulting to freshwater pollution [1]. Synthetic dyes from food, cosmetics, leather, textile industries are a key water contaminant. These dyes are characterized by structural aromatic stability and high recalcitrant to natural degradation, and therefore persistent in water bodies over a long period [2]. The growing concern for clean water sanitation has stimulated the quest effective water treatment methods capable of removing stable synthetic dyes from process industry wastewater [3, 4, 5].

Methylene blue (MB), is a synthetic dye belonging to the thiazine class that has found wide application in pharmaceuticals, biomedicine, and textiles industries. However, despite its widespread use, MB is classified as a persistent organic pollutant that poses serious threats to both ecosystems and human health owing to its hazardous nature, non-biodegradable substance with carcinogenic potential [6, 7]. According to Hamad and Idrus [8], MB is a commonly used as a benchmark contaminant to assess the effectiveness of different adsorption and degradation methods during wastewater treatment research. Numerous researchers have employed diverse techniques including membrane filtration [9], flocculation [10], advanced oxidation [11], photocatalytic degradation, ozonation [12], and biodegradation have been employed for the removal of dye from wastewater [13]. These common methods are associated with some inherent drawbacks such as the complexity in operation and uneconomical of nature of the technology and thus it is necessary to seek efficient and simple dye wastewater treatment methods. Adsorption is considered as an efficient technique for dye contaminant removal due to its advantages such as high efficiency, low cost, simple operation, and insensitive of toxic substances [14]. Different adsorbents have been used for adsorption of MB from wastewater, example include pristine biomass, clay, sludge, biochar and zeolite [15].

Zeolites represent a class of crystalline aluminosilicates characterized by three-dimensional frameworks composed of TO_4 tetrahedra (where T = Si, Al) interconnected through oxygen atoms, forming well-defined cavities and channels of molecular dimensions [16]. These materials possess exceptional properties including high surface area, excellent adsorption capacity, acidic sites, and shape selectivity, rendering them valuable for diverse applications spanning catalysis, ion exchange, adsorption, and separation processes [17]. Among the numerous zeolite frameworks, zeolite-A holds particular significance owing to its low Si/Al ratio, high cation exchange capacity, and well-defined microporous structure. The synthesis of zeolites from natural aluminosilicate (kaolin) sources has attracted considerable attention as a sustainable and economically viable approach. Kaolin, an

Received: 17/04/2026; Revised: 25/04/2026; Accepted: 28/04/2026; Published: 15/05/2026

abundantly available natural clay mineral in Nigeria, serves as an excellent precursor for zeolite synthesis due to its high kaolinite content and favorable Si/Al (~1) ratio [18]. Upon thermal activation to metakaolin, the material becomes reactive toward alkaline hydrothermal treatment, facilitating crystallization into various zeolitic phases [19].

Modification of zeolites through transition metal incorporation has emerged as a promising strategy for enhancing their affinity for target pollutant and adsorption capacity [20]. Iron-modified zeolites, in particular, have garnered significant interest due to their redox activity, catalytic potential in Fenton-like reactions, and capacity to generate reactive oxygen species [21], [22]. Incorporation of iron into adsorbent matrix enables multi-functional adsorption due to the increased the adsorbent surface area [23]. Iron species can be introduced via ion exchange, impregnation, or during synthesis, and may exist as isolated ions, oligomers, or oxide nanoparticles depending on loading levels and preparation methodology [24], [25]. Despite interest in iron-modified zeolites, detailed investigations on the incorporation of iron onto zeolite A derived from a typical Nigerian (Aloji, Kogi State) kaolin for the removal of MB has not been documented to the best of the authors knowledge. The effect of iron modification on the structural, morphological, compositional, and textural properties of the zeolite A framework is also scarcely reported. Although a few studies have reported the application of Iron modification of different zeolites for adsorption of pollutant; examples include Fe doped zeolite from Amazonian kaolinite for methylene blue removal [26], Fe doped zeolite for the removal of tetracycline from aqueous solution [27], Fe doped Saudi natural zeolite for the effective adsorption of methylene blue [28].

This study is therefore aimed at synthesizing zeolite A from Nigerian kaolin via hydrothermal activation, functionalizing it with iron, and comprehensively characterizing the resulting material for its oxide composition, crystalline phase, functional groups present, surface morphology and textural properties with the view of evaluating the iron modified zeolite A potential for MB removal.

2.0 Materials and Methods

2.1 Materials

Raw kaolin sourced from Aloji, Kogi State, Nigeria was used as the aluminosilicate precursor. The clay was collected, packed in polythene bags. Sodium hydroxide (NaOH, ≥98% purity) manufactured by Pure Chems laboratory reagents China, iron (III) chloride hexahydrate ($FeCl_3 \cdot 6H_2O$, ≥97% purity) produced by EMSURE ACS reagent Germany and sodium borohydride ($NaBH_4$ ≥97% purity) manufactured by LOBA CHEMIE PVT China were of analytical grade and used without further purification. Deionized water was employed for all synthesis, washing and solution procedures.

2.2 Method

2.2.1 Preparation of Zeolite-A from Kaolin

The raw kaolin was crushed using a porcelain mortar and pestle to reduce lump sizes and promote homogeneity. The sample was subsequently soaked in deionized water for 12 h at room temperature to disperse aggregated particles and facilitate impurity separation. The suspension was continuously stirred for 30 minutes using a magnetic stirrer to ensure homogeneity. The mixture was then transferred to a 1 L measuring cylinder and allowed to sediment for 2 h. This sedimentation process exploited differential settling rates, permitting the separation of denser quartz and other heavy mineral impurities which accumulated at the bottom, while finer kaolinite particles remained suspended in the supernatant [29]. The supernatant containing purified kaolin was carefully decanted and oven-dried at 100°C for 24 h to constant weight. The dried purified kaolin was then ground into a fine powder using a mortar and pestle and stored in an airtight container for subsequent use.

2.2.2 Synthesis of Zeolite-A from Kaolin

The purified kaolin was thermally activated to transform it into a more reactive amorphous phase (metakaolin). Approximately 20 g of the dried kaolin powder was placed in a ceramic crucible and calcined in a muffle furnace at 850°C for 2 h with a heating rate of 10°C min^{-1} [30]. The resulting metakaolin was allowed to cool naturally to room temperature within a desiccator to prevent moisture absorption. Zeolite-A synthesis was achieved via hydrothermal alkaline activation. In a typical procedure, 6 g of metakaolin was slowly added to 50 mL of 5 M NaOH solution undergoes stirring for 2 h prevent clumping. The resulting slurry was aged at room temperature for 24 h to promote homogeneous nucleation [19]. The aged gel was transferred to a 100 mL Teflon-lined stainless-steel autoclave and subjected to hydrothermal crystallization at 115°C for 5 h. After synthesis, the autoclave was quenched under cold running water to terminate the reaction and washed repeatedly with deionized water until a neutral pH was achieved and finally dried in an oven at 100°C for 8 h to obtain zeolite-A.

Received: 17/04/2026; Revised: 25/04/2026; Accepted: 28/04/2026; Published: 15/05/2026

2.3 Iron Modification of Zeolite-A

Iron functionalization of the synthesized zeolite A was accomplished using impregnation method followed by chemical reduction. 8% (w/v) iron precursor solution was prepared by dissolving 8 g of $FeCl_3 \cdot 6H_2O$ in 100 mL deionized water. Subsequently, 6 g of synthesized zeolite-A was dispersed in 50 mL of the prepared iron solution and stirred continuously for 2 h at room temperature to facilitate maximum iron adsorption onto the zeolite surface and within pore channels [21]. Following impregnation, the iron-loaded zeolite was reduced to introduce zerovalent iron species. A 0.96 M $NaBH_4$ solution was prepared and added to the iron-zeolite suspension under vigorous stirring, which immediately produced black precipitates indicating iron reduction [31]. The mixture was stirred for an additional 30 minutes to ensure complete reduction. The resulting iron-modified zeolite was washed several times with deionized water and ethanol to remove residual chlorides and borates, and dried at 100°C for 8 h. Finally, the dried material was calcined at 400°C for 2 h in a muffle furnace under static air atmosphere to enhance stability and ensure adhesion of iron species to the zeolite support. The resulting iron-modified zeolite was characterized using XRD, FTIR, SEM, and XRF analyses.

2.4 Characterization Techniques

The crystalline phases of the synthesized materials were identified by powder X-ray diffraction (XRD) using a Rigaku D/max-IIIc diffractometer with Cu-Kα radiation (λ = 1.5406 Å) operating at 45 kV and 40 mA. Diffractograms were recorded over a 2θ range of 5–70° with a scan speed of 2° min^{-1}. Fourier transform infrared (FTIR) spectra were obtained using a PerkinElmer 3000 MX spectrometer over the wavenumber range 4000–400 cm^{-1} with a resolution of 4 cm^{-1}, using KBr pellet technique (sample: KBr ratio of 1:100). Surface morphology was examined by scanning electron microscopy (SEM) using a JEOL-JSM 7600F microscope operating at an accelerating voltage of 15 kV; samples were gold-coated prior to analysis to prevent charging. Elemental composition was determined by X-ray fluorescence (XRF) spectrometry using a PANalytical Epsilon 3 spectrometer calibrated with standard reference materials. Textural properties, including specific surface area, pore volume, and pore size distribution, were analyzed by nitrogen adsorption-desorption at 77 K using a Micromeritics ASAP 2020 analyzer. Surface area was calculated using the Brunauer-Emmett-Teller (BET) method in the relative pressure range P/P_0 = 0.005–0.99 cm^3/g. This is consistent with the work of Foroughi et al. [32], while pore size distribution was derived from the desorption branch using the Barrett-Joyner-Halenda (BJH) model.

3.0 Results and Discussion

The results of synthesized and characterization of zeolite and modified zeolites using different techniques such as XRD, XRF, FT-IR, BET and SEM to determine crystal size, oxide compositions, functional group present and surface morphology are presented in Figure 1-4 respectively.

3.1 X-ray Diffraction (XRD) Analysis

The XRD pattern of hydrothermally synthesized zeolite-A in Figure 1 exhibited well-defined crystalline reflections within the Bragg angle of 7.14°, 10.22°, 12.46°, 16.00°, 20.46°, 24.06°, 25.14°, 27.00°, 27.24°, 30.88°, 32.20°, 32.62°, 34.20°, 36.74°, 38.06°, 39.44°, 40.28°, 41.62°, 44.24°, 47.36°, and 49.86°. The synthesized sample displayed distinct peaks characteristic of the zeolite-A lattice. The low-angle peak at 7.14° arises from large interplanar spacings typical of zeolitic materials as reported by [16, 33]. The observation of distinct peaks in this study is consistent with the 7-10° range that signifies an open framework structure as reported by [34]. The peak at 20.46° aligns with approximately 21.7° reported by [35], while the peak at 24.06° matches typical zeolite-A reflections at 23.9-24.0°, confirming successful conversion of metakaolin to the aluminosilicate framework [36]. The crystallite size estimated using Scherrer's equation was approximately 20.74 nm. This value indicates that the hydrothermal conditions promoted extensive, well-ordered crystalline domains through prolonged dissolution-reprecipitation and nucleation processes [37, 38]. The sharp, intense, and symmetric peaks further corroborate high crystallinity [39]. Following iron functionalization, the Fe-doped zeolite-A pattern showed reflections at 7.14°, 10.22°, 12.46°, 16.00°, 20.46°, 24.06°, 25.14, 27.24°, 30.04°, 32.64°, 34.20°, 36.74°, 38.06°, 39.44°, 40.28°, 42.92°, 44.5°, 47.42°, 49.84°, 64.14 and 64.78°. The first seven peaks, closely corresponding to those of synthesized zeolite A, confirm that the primary zeolite A framework remained intact, demonstrating structural stability wherein metal nanoparticles anchor within pores without disrupting the aluminosilicate network [20]. This preservation of the zeolite framework upon iron incorporation is consistent with previous studies on iron-modified zeolites [25, 40]. New reflections at 44.5°, 47.42°, 49.84°, 64.14 and 64.78° indicate modifications arising from iron nanoparticle integration, suggesting slight lattice distortions or the presence of small iron-containing crystallites on the zeolite surface [24, 40]. The crystallite size decreased significantly to 9.06 nm, a common phenomenon when new species are introduced into the crystal matrix, leading to broader peaks and smaller coherent diffraction domains [25, 41]. This reduction aligns with dispersed metal nanoparticles decreasing crystal domain sizes, potentially increasing surface area and enhancing functionality for catalysis, ion exchange and adsorption applications [22].

Received: 17/04/2026; Revised: 25/04/2026; Accepted: 28/04/2026; Published: 15/05/2026

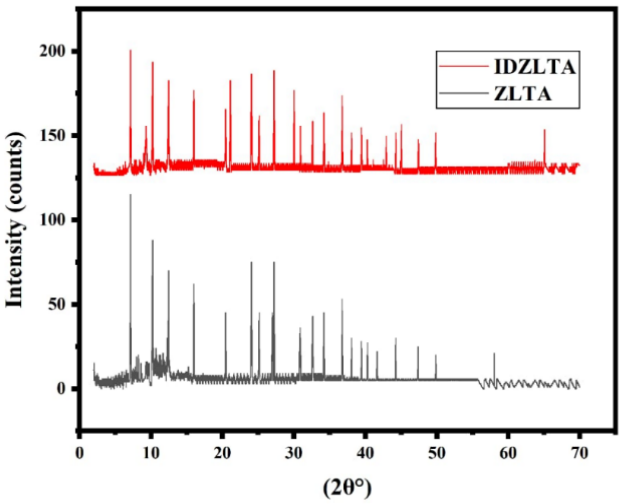

Figure 1. XRD pattern of (a) Zeolite-A and (b) Iron-doped zeolite-A

3.2 Fourier Transform Infrared Spectroscopy (FTIR) Analysis

The FTIR spectrum of synthesized zeolite-A presented in Figure 2 displayed broad O–H stretching bands (3700–3000 cm^{-1}) with peaks at 3724.94 cm^{-1} and 3471–3466 cm^{-1}, corresponding to structural hydroxyl groups and adsorbed water molecules within the zeolite channels [42, 43]. The complementary water-associated band near 1640 cm^{-1} was also evident [44].

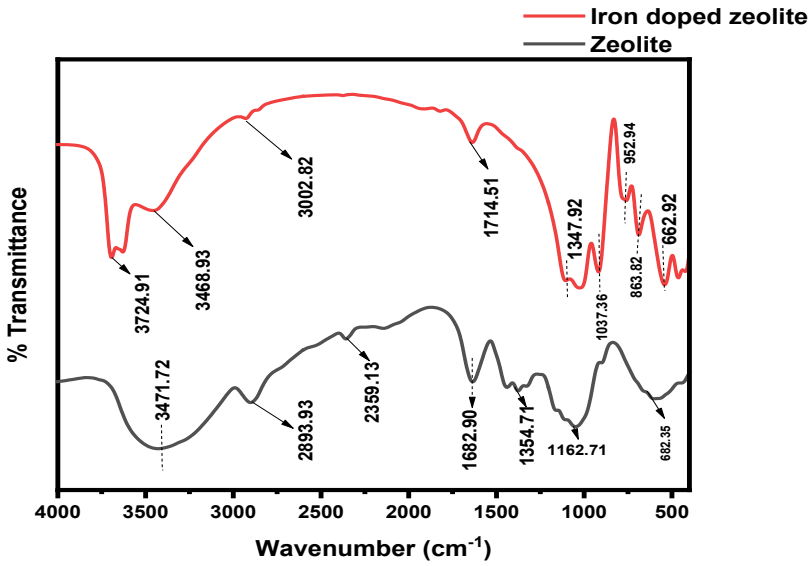

Figure 2. FTIR spectra of (a) Zeolite-A and (b) Iron-doped zeolite-A

In the mid- to low-wavenumber region (1200–400 cm^{-1}), characteristic framework vibrations appeared at 1073 cm^{-1}, 883.82 cm^{-1}, and 602.29 cm^{-1}, confirming the aluminosilicate network [45]. The intense band at 1073 cm^{-1} is assigned to Si–O and Al–O asymmetric stretching (Si–O–T, where T represents tetrahedral Si or Al) [46]. Bands in the 1000–800 cm^{-1} region arise from T–O–T stretching, while the 602 cm^{-1} band corresponds to Si–O–Si or Si–O–Al bending modes. These positions are consistent with established zeolite-A characteristics [47, 48]. The well-defined nature indicates a highly ordered framework resulting from controlled hydrothermal synthesis [49]. Upon iron doping, notable spectral changes occurred. The broad O–H stretching band (3700–3000 cm^{-1}) was retained but exhibited shifts and intensity modifications, indicating altered interactions between hydroxyl groups and incorporated iron species [50]. New absorptions appeared in the 500–600 cm^{-1} region, characteristic of iron–oxygen stretching vibrations, suggesting the presence of nanosized iron oxide clusters or iron atoms interacting with the zeolite matrix [21]. These changes reflect framework preservation alongside additional vibrational features arising from iron integration [51], [25]. Critically, the persistence of fundamental Si–O and Al–O bands confirms that the zeolite-A framework remains intact after doping [52, 53]. The iron addition introduces functional complexity without disrupting the aluminosilicate network. The zeolite-A spectrum exhibits characteristic

Received: 17/04/2026; Revised: 25/04/2026; Accepted: 28/04/2026; Published: 15/05/2026

hydroxyl and framework vibrations consistent with reported literature [54], while new Fe–O bands and modified OH regions confirm iron incorporation with preservation of the underlying framework structure [55].

3.3 Scanning Electron Microscopy (SEM) Analysis

The SEM micrograph of synthesized zeolite-A in Figure 3a revealed well-developed, faceted crystals with a characteristic cubic to polyhedral morphology and distinct "blocky" shape. This microstructure, comprising micrometer-scale solid polyhedral crystals, is typical of hydrothermally synthesized zeolite-A [56]. The observed cubic form with mixed smooth and rugged surface textures agrees with reported zeolite A type morphologies [57]. This polyhedral habit results from the corner-sharing arrangement of SiO_4 and AlO_4 tetrahedra during crystallization [58]. Following iron doping, the SEM image in Figure 3b exhibited distinct morphological changes. The material showed smaller, aggregated particles with a noticeably rougher surface compared to pristine zeolite-A; this observation is consistent with the result of [59]. This textured appearance is attributed to nanoscale iron particles likely Fe^0 deposited onto the zeolite crystal surfaces [31, 60]. While the fundamental zeolite crystal form is preserved, the surface becomes coated with nanometer-sized particles, confirming successful metal incorporation [61]. These increased surface irregularities in the Fe-doped sample suggest enhanced active site availability, potentially beneficial for catalytic and adsorption applications [62]. Similar morphological observations have been reported for iron-modified zeolites, wherein metal oxide nanoparticles coat the zeolite surface while preserving the underlying framework structure [21, 25].

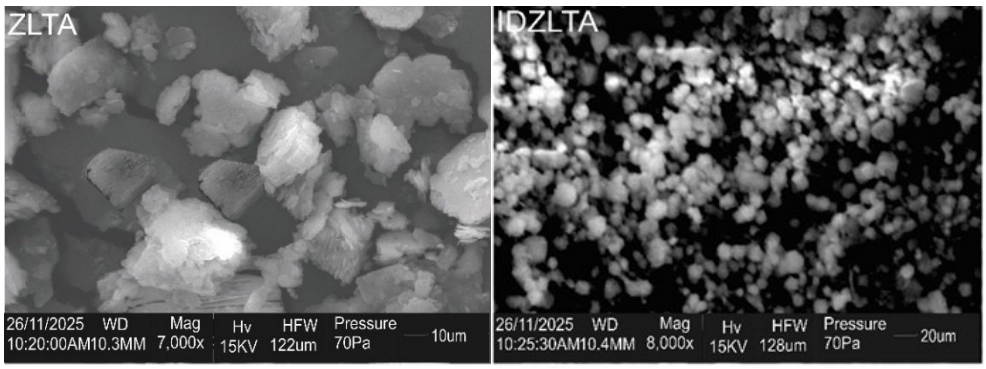

Figure 3. SEM images of (a) Zeolite-A and (b) Iron-doped zeolite-A

3.4 X-ray Fluorescence (XRF) Analysis

XRF results presented in Table 1 confirmed framework modification following iron incorporation into zeolite-A. Parent zeolite-A exhibited the expected zeolite A composition, with high SiO_2 (49.71 wt.%) and Al_2O_3 (30.94 wt.%) concentrations confirming its aluminosilicate framework [63]. The Si/Al molar ratio of 1.36 indicates low-silica composition, correlating with high framework charge density and cation exchange capacity. Na_2O (8.15 wt.%) confirms the sodium form of the zeolite A structure, while additional constituents include CaO (3.47 wt.%), Fe_2O_3 (2.26 wt.%), and trace oxides.

Table 1. Chemical composition (wt.%) of zeolite-A and iron-modified zeolite

Oxide	Zeolite A	Iron-doped zeolite A
SiO_2	49.71	55.50
Al_2O_3	30.94	24.90
Fe_2O_3	2.26	9.83
MnO	0.02	0.14
CaO	3.47	2.25
P_2O_5	0.07	0.27
K_2O	0.06	0.60
TiO_2	1.67	1.29
MgO	0.28	2.31
Na_2O	8.15	-
Cr_2O_3	0.20	0.03
NiO	0.10	0.02
CuO	0.01	-
LOI	2.24	2.22
Total	**99.48**	**100**

Received: 17/04/2026; Revised: 25/04/2026; Accepted: 28/04/2026; Published: 15/05/2026

This finding is consistent with the observation of [46]. Upon iron doping, Fe_2O_3 concentration increased from 2.26 wt.% to 9.83 wt.%, confirming successful incorporation. Concurrently, Al_2O_3 decreased to 24.90 wt.% while SiO_2 increased to 55.20 wt.%, yielding an elevated Si/Al ratio of 1.89. The observable rise in silica ratio for the Fe incorporated zeolite is consistent with the work of [64]. The complete absence of Na_2O in the doped sample strongly supports Na^+ replacement by Fe^{3+} within zeolite A cavities [65]. The slight MgO increase (2.31 wt.%) suggests minor impurity effects rather than structural substitution [66]. LOI values of 2.24% (zeolite-A) and 2.22% (doped) correspond to adsorbed water and structural hydroxyl groups typical of zeolites; the slight reduction after doping may indicate partial dehydration or decreased hydrophilicity resulting from iron incorporation [67]. The increased Fe_2O_3 content and Si/Al ratio carry functional significance: iron species introduce active sites for redox-catalytic or Fenton-like reactions, while the higher Si/Al ratio enhances hydrothermal stability, albeit with reduced cation exchange capacity [68]. Similar compositional trends have been observed in iron-modified zeolites prepared by impregnation methods [69, 25].

3.5 BET Analysis

The textural properties of the iron-doped zeolite-A were investigated by nitrogen physisorption at 77 K. Figure 4 presents the nitrogen adsorption-desorption isotherm, and the corresponding textural parameters specific surface area, total pore volume, and average pore width are summarized in Table 2. For pure zeolite A, BET analysis gave a surface area of 515.22 m^2/g, a total pore volume of 0.4402 cm^3/g, and an average pore width of 3.033 nm. After Fe doping, the specific surface area decreased to 380.35 m^2/g (≈26% reduction), while the total pore volume slightly increased to 0.4522 cm^3/g and the average pore width narrowed to 2.855 nm. These values reflect a high surface area material that combines inherent zeolite microporosity with an additional mesoporous contribution which is consistent with the results obtained by [70, 71].

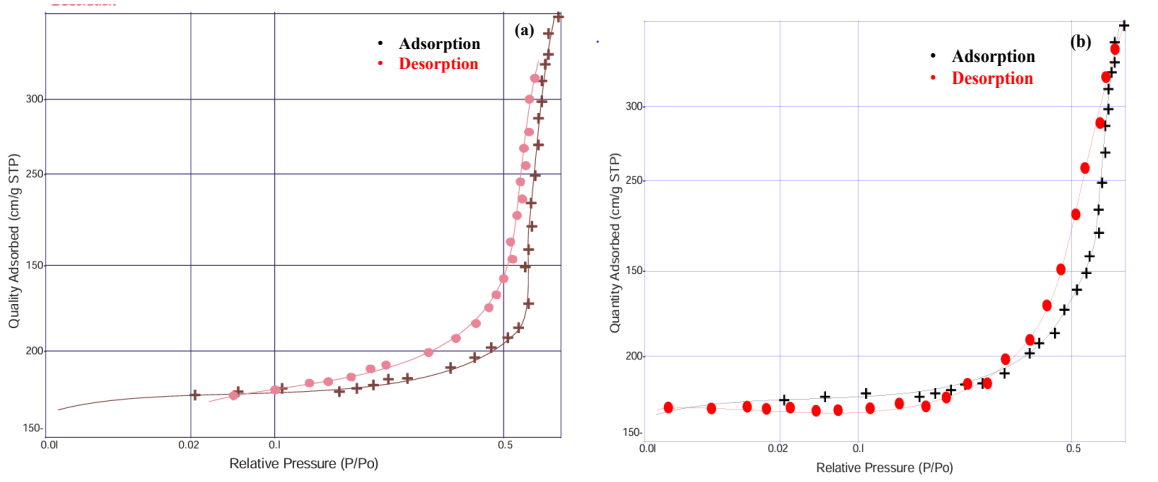

Figure 4. BET adsorption-desorption isotherm of Zeolite A and iron-doped zeolite

Table 2. Textural properties of zeolite A and iron doped zeolite A

Parameter	Zeolite A	Fe doped Zeolite A
BET Surface Area ($m^2\ g^{-1}$)	515.220	380.350
Total Pore Volume ($cm^3\ g^{-1}$)	0.440200	0.4522
Average Pore Width (nm)	3,033	2.855
Isotherm Type	Type IV	Type IV
Hysteresis Loop Type	Type H4	Type H3

The measured surface area (380.35 m^2/g) falls within the lower range reported for zeolite A (300–600 m^2/g) [72]. This reduction following iron impregnation is commonly observed in Fe-modified zeolites and is attributed to partial pore blockage, active site occupation, or structural perturbations [69]. The value indicates a partially pore-occupied system wherein iron species reside within surface cavities or near pore entrances, reducing accessible microporous area while retaining significant adsorption capacity [73]. Similar surface area reductions upon metal incorporation have been widely reported for iron-modified zeolites [21, 25].

Interestingly, the total pore volume remained nearly unchanged despite the surface area loss. This observation, together with the decrease in average pore width, suggests that Fe species primarily narrow the pores rather than completely blocking them. The increased pore volume relative to pure microporous zeolite A likely arises from dispersed iron nanoparticle clusters on zeolite surfaces rather than from structural collapse. As indicated by the

Received: 17/04/2026; Revised: 25/04/2026; Accepted: 28/04/2026; Published: 15/05/2026

XRD crystallite size reduction from 20.74 nm to 9.06 nm, the dispersed iron nanoparticles disrupt the close packing of zeolite crystals, generating additional inter particle voids [74]. Velty and Corma [17] added that iron incorporation into zeolite can generate additional mesoporosity in zeolitic materials. The coexistence of microporous cavities and mesoporous secondary structures benefits adsorption and catalytic applications. In this iron doped system, Fe^0 or iron oxide species provide additional active sites for pollutant adsorption [22, 25]. The relatively high surface area and pore volume demonstrate that metal incorporation creates a hierarchical structure without compromising the zeolite framework, a feature advantageous for adsorption applications. The nitrogen adsorption/desorption isotherm displayed in Figure 4 exhibited Type IV behavior (IUPAC classification) with a visible hysteresis loop of Type H3 loop confirming mesoporosity alongside inherent zeolite microporosity. [75].

3.6 Batch Adsorption of MB using Zeolite A and Fe-doped Zeolite A

3.6.1 Effect of initial concentration

The initial concentration plays a key role in the removal of MB from aqueous solutions. In this study, the initial MB concentration was varied from 6 to 30 mg/L as presented in Figure 5. The results show that as the initial MB concentration increased from 6 to 30 mg/L, the percentage MB removed decreases negligibly as from 98 to 97% for zeolite A as against 100 to 88% when Fe-doped zeolite was employed for adsorption under same condition. The observation in this study is consistent with 90% percentage MB removal under similar condition using Fe-zeolites from Amazonian kaolinite as reported by [26]. This present study demonstrates that the initial concentration of 6 mg/L is optimum for MB removal. The reduction in percentage MB removal at higher dye concentrations > 6 mg/L is probably attributed to the saturation of adsorption sites on the adsorbent surface. Earlier studies have reported that at elevated concentrations the adsorbent active sites become easily occupied due to limited interaction of the dye molecules with the adsorbent surface [76, 77].

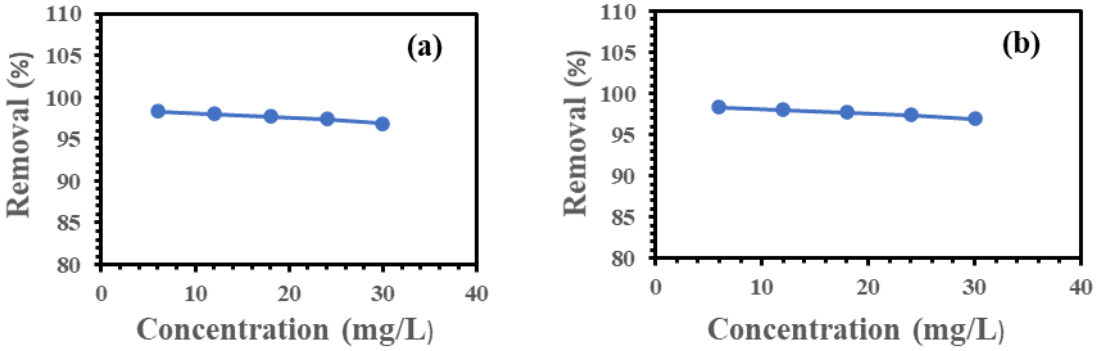

Figure 5. Effect of initial concentration on the removal of methylene blue (MB) by (a) zeolite A and (b) Fe Doped zeolite A

3.6.2 Effect of adsorbent dosage

In adsorption studies, the adsorbent dosage is a critical variable that must be optimized to ensure the highest possible adsorption efficiency. Figure 6 shows the effect of adsorbent dosage on the adsorption of MB by varying adsorbent dosage from 0.2 to 1.2 g keeping all other variable constant at equilibrium condition. According to Figure 6a the adsorption of methylene blue (MB) increased from 92.4 to 96.7% as the dosage increased from 0.2 to 0.8g after which there was no significant increase in adsorption as the value remained nearly constant (97%).

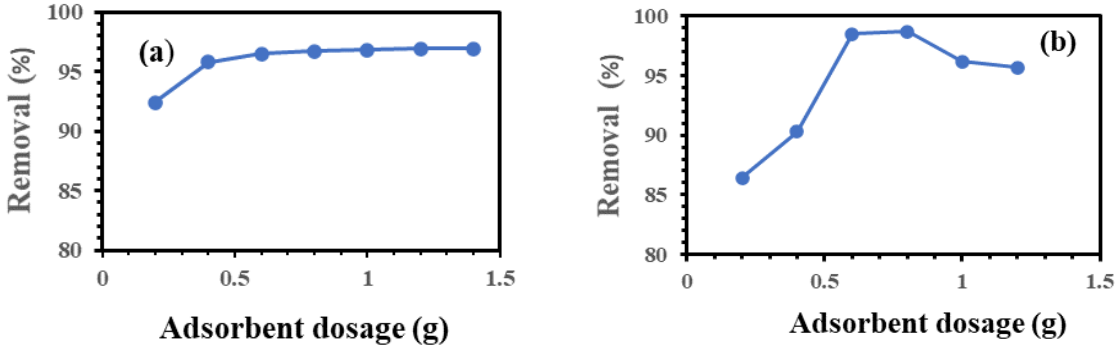

Figure 6. Effect of adsorbent dosage on the removal of methylene blue (MB) by (a) zeolite A and (b) Fe doped zeolite

In the case of the Fe-doped zeolite, the adsorption of methylene blue (MB) increased swiftly from 86.4 to 99% as the dosage increased from 0.2 to 0.6 g thereafter no significant change was recorded as the dosage was

Received: 17/04/2026; Revised: 25/04/2026; Accepted: 28/04/2026; Published: 15/05/2026

increased to 0.8 g, further increase in dosage resulted in decrease in percentage MB removal (Figure 6b). These findings suggest that increase in adsorbent dosage beyond 0.6 g has no significant effect on the MB removal due to saturation of the active sites. According to Al-Asadi et al. [78] the high adsorption observed can be attributed to the higher adsorbent surface area and corresponding adsorption sites. The optimum adsorbent dosage for Fe-doped zeolite was 0.6 g, yielding 99% removal efficiency. In contrast, zeolite A required a higher optimum dosage of 0.8 g to achieve 97% removal, demonstrating clearly the greater adsorption capacity for the Fe-doped zeolite.

3.6.3 Effect of contact time

Establishing the optimal contact time required to reach adsorption equilibrium is crucial for maximizing methylene blue (MB) removal efficiency. Figure 7 illustrates the effect of contact time on MB removal over a range of 30 to 120 minutes to determine the optimum equilibrium time for MB removal

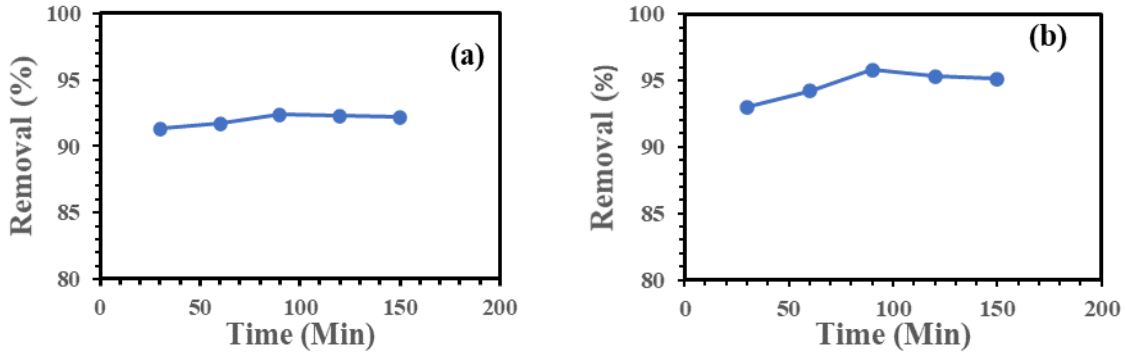

Figure 7. Effect of contact time on the removal of methylene blue (MB) by (a) zeolite A and (b) Fe doped zeolite A

Figure 7 revealed that the MB removal efficiency using zeolite A increased fairly from 91.3 to 92.4% as the contact time was varied from 30 to 90 minutes, after which no significant further adsorption was observed. In contrast, the iron doped zeolite A exhibited a more pronounced increase, from 93 to 96% under same condition. The observation suggests that the Fe-doped zeolite exhibited a higher adsorption of MB. This finding aligns with the work of Saod et al. [79], who reported ≥90% MB removal across all tested contact times (15–120 min). According to Rehman et al. [80], the enhanced adsorption can be attributed to the higher surface area and greater availability of vacant active sites on the adsorbent. Based on these results, a contact time of 90 minutes was selected as the optimal equilibrium time.

4.0 Conclusion

This study successfully synthesized phase-pure zeolite-A from Nigerian kaolin via hydrothermal activation, followed by iron functionalization. Characterization confirmed a well-crystalline LTA framework (crystallite size 20.74 nm) that remained intact after iron doping, with Fe_2O_3 content increasing from 2.26 to 9.83 wt.% and Si/Al ratio rising from 1.36 to 1.89. The iron-modified zeolite exhibited a BET surface area of 380.35 m^2/g, Type IV isotherm, and Type H3 hysteresis loop, confirming hierarchical micro-mesoporosity. Batch adsorption achieved 99.6% methylene blue removal under optimized conditions (6 mg/L, 0.6 g dosage, 90 min, pH 6), outperforming unmodified zeolite A (98.3%) with a lower optimum dosage. This work positions iron-modified zeolite-A from Nigerian kaolin as a high-performance adsorbent for cationic dye removal in textile wastewater treatment. Further study should explore the optimization of effect of process variables using response surface methodology and Artificial Neural network. Isotherm, kinetic and thermodynamics of MB adsorption should also be explicitly investigated.

Acknowledgments

The authors thankfully appreciate the support of Africa Centre of Excellence for Mycotoxin and Food Safety (ACEMFS) for providing access to their laboratory.

References

[1] J. Lin, W. Ye, M. Xie, D. H. Seo, J. Luo, Y. Wan, and B. Van der Bruggen, "Environmental impacts and remediation of dye-containing wastewater," *Nature Reviews Earth & Environment*, vol. 4, no. 11, pp. 785–803, 2023.

[2] M. Tripathi, S. Singh, S. Pathak, J. Kasaudhan, A. Mishra, S. Bala, D. Garg, D. Singh, R. Singh, and N. Pathak, "Recent strategies for the remediation of textile dyes from wastewater: A systematic review," *Toxics*, vol. 11, no. 11, p. 940, 2023.

[3] T. Shindhal, P. Rakholiya, S. Varjani, A. Pandey, H. H. Ngo, W. Guo, Y. Ng, and M. J. Taherzadeh, "A critical review on advances in the practices and perspectives for the treatment of dye industry wastewater," *Bioengineered*, vol. 12, no. 1, pp. 70–87, 2021.
[4] Y. Kuang, X. Zhang, and S. Zhou, "Adsorption of methylene blue in water onto activated carbon by surfactant modification," *Water*, vol. 12, no. 2, p. 587, 2020.
[5] S. H. Kim, J. I. Park, S. Lee, H. R. An, H. Kim, B. Son, J. Lee, S. Bae, and H. U. Lee, "Enhancing adsorption efficiency for environmentally-friendly removal of As(V) and Pb(II) using a biochar-iron oxide composite," *Applied Surface Science*, vol. 667, p. 160348, 2024.
[6] I. Khan, K. Saeed, I. Zekker, B. Zhang, A. H. Hendi, A. Ahmad, S. Ahmad, N. Zada, H. Ahmad, L. A. Shah, T. Shah, and I. Khan, "Review on methylene blue: Its properties, uses, toxicity and photodegradation," *Water*, vol. 14, no. 2, p. 242, 2022.
[7] T. Islam, M. R. Repon, T. Islam, Z. Sarwar, and M. M. Rahman, "Impact of textile dyes on health and ecosystem: A review of structure, causes, and potential solutions," *Environmental Science and Pollution Research*, vol. 30, no. 4, pp. 9207–9242, 2023.
[8] S. Hamad and S. Idrus, "Recent developments in the application of bio-waste-derived adsorbents for the removal of methylene blue from wastewater: A review," *Polymers*, vol. 14, no. 4, p. 783, 2022.
[9] S. P. Bera, M. Godhaniya, and C. Kothari, "Emerging and advanced membrane technology for wastewater treatment: A review," *Journal of Basic Microbiology*, vol. 62, no. 3–4, pp. 245–259, 2022.
[10] W. Mnif and F. Ben Rebah, "Bioflocculants as alternative to synthetic polymers to enhance wastewater sludge dewaterability: A review," *Energies*, vol. 16, no. 8, p. 3392, 2023.
[11] A. Ponnusami, S. Sinha, H. Ashokan, M. V. Paul, S. P. Hariharan, J. Arun, K. P. Gopinath, Q. Hoang Le, and A. Pugazhendhi, "Advanced oxidation process (AOP) combined biological process for wastewater treatment: A review on advancements, feasibility and practicability of combined techniques," *Environmental Research*, vol. 237, p. 116944, 2023.
[12] E. Kordouli, K. Bourikas, A. Lycourghiotis, and C. Kordulis, "The mechanism of azo-dyes adsorption on the titanium dioxide surface and their photocatalytic degradation over samples with various anatase/rutile ratios," *Catalysis Today*, vol. 252, pp. 128–135, 2015.
[13] T. Shindhal, P. Rakholiya, S. Varjani, A. Pandey, H. H. Ngo, W. Guo, Y. Ng, and M. J. Taherzadeh, "A critical review on advances in the practices and perspectives for the treatment of dye industry wastewater," *Bioengineered*, vol. 12, no. 1, pp. 70–87, 2021.
[14] R. Rashid, I. Shafiq, P. Akhter, M. J. Iqbal, and M. Hussain, "A state-of-the-art review on wastewater treatment techniques: The effectiveness of adsorption method," *Environmental Science and Pollution Research*, vol. 28, no. 8, pp. 9050–9066, 2021.
[15] Y. Kuang, X. Zhang, and S. Zhou, "Adsorption of methylene blue in water onto activated carbon by surfactant modification," *Water*, vol. 12, no. 2, p. 587, 2020.
[16] W. J. Roth, T. Sasaki, K. Wolski, B. Gil, S. Zapotoczny, J. Čejka, M. Kubů, M. Mazur, Y. Ebina, N. Sakai, D. M. Tang, and R. Ma, "Exfoliating layered zeolite MFI into unilamellar nanosheets in solution as precursors for the synthesis of hierarchical nanocomposites and oriented films," *Inorganic Chemistry Frontiers*, vol. 10, no. 5, pp. 1511–1521, 2023.
[17] A. Velty and A. Corma, "Advanced zeolite and ordered mesoporous silica-based catalysts for the conversion of CO_2 to chemicals and fuels," *Chemical Society Reviews*, vol. 52, no. 5, pp. 1773–1946, 2023.
[18] V. C. Eluwa, A. S. Kovo, A. S. Abdulkareem, J. O. Tijani, and S. Mustapha, "Hydrothermal synthesis of kaolin-based zeolite A for use in the deodourisation of poultry litter," *Next Research*, vol. 2, no. 3, p. 100443, 2025.
[19] E. Nyankson, J. K. Efavi, A. Yaya, G. Manu, K. Asare, J. Daafuor, and R. Y. Abrokwah, "Synthesis and characterisation of zeolite-A and Zn-exchanged zeolite-A based on natural aluminosilicates and their potential applications," *Cogent Engineering*, vol. 5, no. 1, 2018.
[20] H. Wang, L. Wang, and F.-S. Xiao, "Metal@zeolite hybrid materials for catalysis," *ACS Central Science*, vol. 6, no. 10, pp. 1685–1697, 2020.
[21] J. Zhang, X. Tang, H. Yi, Q. Yu, Y. Zhang, J. Wei, and Y. Yuan, "Synthesis, characterization and application of Fe-zeolite: A review," *Applied Catalysis A: General*, vol. 630, p. 118467, 2021.
[22] K. Solanki, S. Sharma, S. Yadav, B. Kaushik, P. Rana, R. Dixit, and R. K. Sharma, "Hierarchical 3D flower like metal oxides micro/nanostructures: Fabrication, surface modification, their crucial role in environmental decontamination, mechanistic insights, and future perspectives," *Small*, vol. 19, no. 26, 2023.
[23] S. H. Kim, J. I. Park, S. Lee, H. R. An, H. Kim, B. Son, J. Lee, S. Bae, and H. U. Lee, "Enhancing adsorption efficiency for environmentally-friendly removal of As(V) and Pb(II) using a biochar-iron oxide composite," *Applied Surface Science*, vol. 667, p. 160348, 2024.

Received: 17/04/2026; Revised: 25/04/2026; Accepted: 28/04/2026; Published: 15/05/2026

[24] M. Saifuddin, J. Bae, and K. S. Kim, "Role of Fe, Na and Al in Fe-zeolite-A for adsorption and desorption of phosphate from aqueous solution," *Water Research*, vol. 158, pp. 246–256, 2019.
[25] G. M. dos Santos, M. F. Paiva, J. O. C. de França, S. C. L. Dias, and J. A. Dias, "Synthesis and properties of *BEA zeolite modified with iron (III) oxide," *Inorganics*, vol. 13, no. 12, 2025.
[26] V. A. A. de Freitas, D. de Souza Pinheiro, C. F. Peixoto, L. C. A. de Oliveira, and P. R. da Costa Couceiro, "Synthesis of Fe-zeolites from Amazonian kaolinite for methylene blue removal: Adsorption and photocatalytic activity," *Dalton Transactions*, 2025.
[27] M. H. Jannat Abadi, S. M. M. Nouri, R. Zhiani, H. D. Heydarzadeh, and A. Motavalizadehkakhky, "Removal of tetracycline from aqueous solution using Fe-doped zeolite," *International Journal of Industrial Chemistry*, vol. 10, no. 4, pp. 291–300, 2019.
[28] M. Alsuhybani, S. Alshehri, A. Alquwaizany, E. Alosime, R. Alaeq, and A. Alrehaili, "Effective adsorption of methylene blue using natural Saudi zeolite as a low-cost sustainable adsorbent," *Scientific Reports*, vol. 16, no. 1, p. 211, 2026.
[29] O. B. Al-Ameri, M. Alzuhairi, E. Bailón-García, F. Carrasco-Marín, and J. Amaro-Gahete, "Transforming petrochemical processes: Cutting-edge advances in kaolin catalyst fabrication," *Applied Sciences*, vol. 14, no. 19, p. 9080, 2024.
[30] V. C. Eluwa, P. A. Obasa, M. Esther, and C. A. Igbonekwu, "Synthesis and characterization of zeolite A from Aloji kaolin via hydrothermal method," *Journal of Materials Science Research and Reviews*, vol. 7, no. 4, pp. 592–601, 2024.
[31] A. Mekki, A. Mokhtar, M. Hachemaoui, M. Beldjilali, M. F. Meliani, H. H. Zahmani, and B. Boukoussa, "Fe and Ni nanoparticles-loaded zeolites as effective catalysts for catalytic reduction of organic pollutants," *Microporous and Mesoporous Materials*, vol. 310, p. 110597, 2021.
[32] M. Foroughi, A. Salem, and S. Salem, "Characterization of phase transformation from low grade kaolin to zeolite LTA in fusion technique: Focus on quartz melting and crystallization in presence of $NaAlO_2$," *Materials Chemistry and Physics*, vol. 258, p. 123892, 2021.
[33] M. M. Treacy and J. B. Higgins, *Collection of Simulated XRD Powder Patterns for Zeolites*, 5th ed. Amsterdam, The Netherlands: Elsevier, 2007.
[34] X. Guo and A. Navrotsky, "Hydration dynamics in zeolite A – An X-ray diffraction and infrared spectroscopic study," *Microporous and Mesoporous Materials*, vol. 268, pp. 197–201, 2018.
[35] M. K. Król and P. Jeleń, "The effect of heat treatment on the structure of zeolite A," *Materials*, vol. 14, no. 16, pp. 1–9, 2021.
[36] N. A. Sholeha, L. Jannah, H. N. Rohma, N. Widiastuti, D. Prasetyoko, A. A. Jalil, and H. Bahruji, "Synthesis of zeolite NaY from dealuminated metakaolin as Ni support for CO_2 hydrogenation to methane," *Clays and Clay Minerals*, vol. 68, no. 5, pp. 513–523, 2020.
[37] W. Nzodom Djozing, S. Valange, S. I. Nikitenko, and T. Chave, "Sonohydrothermal synthesis of zeolite A and its phase transformation into sodalite," *Dalton Transactions*, vol. 53, no. 39, pp. 16407–16421, 2024.
[38] A. Khaleque, M. M. Alam, M. Hoque, S. Mondal, J. B. Haider, B. Xu, M. A. H. Johir, A. K. Karmakar, J. L. Zhou, M. B. Ahmed, and M. A. Moni, "Zeolite synthesis from low-cost materials and environmental applications: A review," *Environmental Advances*, vol. 2, Nov. 2020.
[39] N. Hijazi, A. Bavykina, I. Yarulina, T. Shoinkhorova, E. V. Ramos-Fernandez, and J. Gascon, "Chemical engineering of zeolites: Alleviating transport limitations through hierarchical design and shaping," *Chemical Society Reviews*, vol. 54, no. 13, pp. 6335–6384, 2025.
[40] J. Zhang, X. Tang, H. Yi, Q. Yu, and Y. Zhang, "Synthesis, characterization and application of Fe-zeolite: A review," *Applied Catalysis A: General*, vol. 630, p. 118467, 2022.
[41] J. Greasley and P. Hosein, "Exploring supervised machine learning for multi-phase identification and quantification from powder X-ray diffraction spectra," *Journal of Materials Science*, vol. 58, no. 12, pp. 5334–5348, 2023.
[42] G. N. Vayssilov, H. A. Aleksandrov, E. Dib, I. M. Costa, N. Nesterenko, and S. Mintova, "Superacidity and spectral signatures of hydroxyl groups in zeolites," *Microporous and Mesoporous Materials*, vol. 343, p. 112144, 2022.
[43] H. Eren, F. N. Türk, and H. Arslanoğlu, "Synthesis of zeolite from industrial wastes: A review on characterization and heavy metal and dye removal," *Environmental Science and Pollution Research International*, vol. 31, no. 29, pp. 41791–41823, 2024.
[44] R. L. White, "A temperature perturbation infrared spectroscopy comparison of HY and NaY zeolite dehydration/rehydration," *Minerals*, vol. 14, no. 1, p. 104, 2024.
[45] M. Król, A. Koleżyński, and W. Mozgawa, "Vibrational spectra of zeolite Y as a function of ion exchange," *Molecules*, vol. 26, no. 2, p. 342, 2021.

Received: 17/04/2026; Revised: 25/04/2026; Accepted: 28/04/2026; Published: 15/05/2026

[46] Y. K. Ma, S. Rigolet, L. Michelin, J. L. Paillaud, S. Mintova, F. Khoerunnisa, T. J. Daou, and E. P. Ng, "Facile and fast determination of Si/Al ratio of zeolites using FTIR spectroscopy technique," *Microporous and Mesoporous Materials*, vol. 311, 2021.
[47] J. A. Schott, C.-L. Do-Thanh, W. Shan, N. G. Puskar, S. Dai, and S. M. Mahurin, "FTIR investigation of the interfacial properties and mechanisms of CO_2 sorption in porous ionic liquids," *Green Chemical Engineering*, vol. 2, no. 4, pp. 392–401, 2021.
[48] S. Pasieczna-Patkowska, M. Cichy, and J. Flieger, "Application of Fourier transform infrared (FTIR) spectroscopy in characterization of green synthesized nanoparticles," *Molecules*, vol. 30, no. 3, pp. 1–36, 2025.
[49] D. Benedis, "Surface characterization of zeolite by nanoscale IR spectroscopy," Ph.D. dissertation, Université Paris-Saclay, 2023.
[50] R. Jain and S. Gulati, "Influence of Fe^{2+} substitution on FTIR and Raman spectra of Mn ferrite nanoparticles," *Vibrational Spectroscopy*, vol. 126, p. 103540, 2023.
[51] F. C. Rivas, I. Rodríguez-Iznaga, G. Berlier, D. T. Ferro, B. Concepción-Rosabal, and V. Petranovskii, "Fe speciation in iron modified natural zeolites as sustainable environmental catalysts," *Catalysts*, vol. 9, no. 10, pp. 1–14, 2019.
[52] W. A. Albuquerque, A. J. N. Filho, Y. Romaguera-Barcelay, S. Medina-Carrasco, M. del M. Orta, P. Trigueiro, and R. R. Peña-Garcia, "Synergistic ZnO–CuO/halloysite nanocomposite for photocatalytic degradation of ciprofloxacin with high stability and reusability," *Minerals*, vol. 15, no. 9, pp. 1–21, 2025.
[53] V. A. Reyes Villegas, J. I. De León Ramirez, L. Pérez-Cabrera, S. Pérez-Sicairos, R. I. Yocupicio-Gaxiola, J. R. Chávez-Méndez, L. Huerta-Arcos, and V. Petranovskii, "Sonochemical post-synthesis modification of Y zeolite with iron species," *Materials Chemistry and Physics*, vol. 331, p. 130199, 2025.
[54] G. Jalloul, N. Hijazi, C. Boyadjian, H. Awala, A. B. Albadarin, and M. N. Ahmad, "Titania-zeolite composite for tetracycline photocatalytic degradation under visible light: A comparison between doping and ion exchange," *Heliyon*, vol. 10, no. 11, p. e31854, 2024.
[55] C. Wan, X. Cui, M. Liu, B. Xu, J. Sun, and S. Bai, "Structure features and physicochemical performances of Fe-containing clinoptilolites obtained via the aqueous exchange of the balanced cations and isomorphs substitution of the heulandite skeletons for electrocatalytic activity of oxygen evolution reaction and adsorptive performance of CO_2," *Molecules*, vol. 28, no. 7, p. 2889, 2023.
[56] D. D. Athayde, G. M. dos Santos, A. C. B. de Faria, C. de Lima Ribeiro, C. M. Aiube, D. A. A. Ladislau, E. Paulo da Silva, L. F. de Sousa Lima, R. N. de Souza, S. L. Pereira da Silva, N. D. S. Mohallem, and A. M. A. Silva, "Investigation of the reaction time and hydrothermal synthesis route on the SSZ-13 zeolite particle crystallization and CO_2 adsorption," *Microporous and Mesoporous Materials*, vol. 384, p. 113428, 2025.
[57] J. Mokrzycki, W. Franus, R. Panek, M. Sobczyk, P. Rusiniak, J. Szerement, R. Jarosz, L. Marcińska-Mazur, T. Bajda, and M. Mierzwa-Hersztek, "Zeolite composite materials from fly ash: An assessment of physicochemical and adsorption properties," *Materials*, vol. 16, no. 6, 2023.
[58] J.-Q. Zhong and H.-J. Freund, "Two-dimensional ultrathin silica films," *Chemical Reviews*, vol. 122, no. 13, pp. 11172–11246, 2022.
[59] M. R. Adam, M. H. D. Othman, S. H. S. A. Kadir, M. N. M. Sokri, Z. S. Tai, Y. Iwamoto, M. Tanemura, S. Honda, M. H. Puteh, M. A. Rahman, and J. Jaafar, "Influence of the natural zeolite particle size toward the ammonia adsorption activity in ceramic hollow fiber membrane," *Membranes*, vol. 10, no. 4, pp. 1–18, 2020.
[60] S. Vohl, I. Ban, J. Stergar, and M. Slemnik, "Synthesis, characterization, and application of magnetic zeolite nanocomposites: A review of current research and future applications," *Nanomaterials*, vol. 15, no. 12, 2025.
[61] E. Shafia, S. Esposito, M. Manzoli, M. Chiesa, P. Tiberto, G. Barrera, G. Menard, P. Allia, F. Freyria, E. Garrone, and B. Bonelli, "Al/Fe isomorphic substitution versus Fe_2O_3 clusters formation in Fe-doped aluminosilicate nanotubes (imogolite)," *Journal of Nanoparticle Research*, vol. 17, 2015.
[62] P. V. Mane, R. M. Rego, P. L. Yap, D. Losic, and M. D. Kurkuri, "Unveiling cutting-edge advances in high surface area porous materials for the efficient removal of toxic metal ions from water," *Progress in Materials Science*, vol. 146, p. 101314, 2024.
[63] O. A. Ajayi, S. S. Adefila, and M. T. Ityokumbul, "Organic template free synthesis of ZSM11 from kaolinite clay," *Nigerian Journal of Technology*, vol. 36, no. 2, p. 444, 2017.
[64] Z. Tauanov and V. J. Inglezakis, "Removal of iodide from water using silver nanoparticles-impregnated synthetic zeolites," *Science of the Total Environment*, vol. 682, pp. 259–270, 2019.
[65] P. Pasabeyoglu, G. Moumin, L. de Oliveira, M. Roeb, and B. Akata, "Solarization of the zeolite production: Calcination of kaolin as proof-of-concept," *Journal of Cleaner Production*, vol. 414, p. 137611, 2023.
[66] N. B. T. Tran, N. B. Duong, and N. L. Le, "Synthesis and characterization of magnetic Fe_3O_4/zeolite NaA nanocomposite for the adsorption removal of methylene blue potential in wastewater treatment," *Journal of Chemistry*, vol. 2021, p. 6678588, 2021.

Received: 17/04/2026; Revised: 25/04/2026; Accepted: 28/04/2026; Published: 15/05/2026

[67] A. Mamudu, M. Emetere, D. Okocha, S. Taiwo, F. Ishola, F. Elehinafe, and E. Okoro, "Parametric investigation of indigenous Nigeria mineral clay (kaolin and bentonite) as a filler in the fluid catalytic cracking unit (FCCU) of a petroleum refinery," *Alexandria Engineering Journal*, vol. 59, no. 6, pp. 5207–5217, 2020.
[68] E. Svobodová, Z. Tišler, K. Peroutková, K. Strejcová, J. Abrham, J. Šimek, Z. Gholami, and M. Vakili, "Adsorption of Cu(II) and Ni(II) from aqueous solutions using synthesized alkali-activated foamed zeolite adsorbent: Isotherm, kinetic, and regeneration study," *Molecules*, vol. 29, no. 10, 2024.
[69] S. J. S. Xavier, M. A. Klunk, and N. R. Caetano, "Advances in the use of zeolites for industrial effluent treatment and carbon dioxide mitigation: A review," *Applied Sciences*, vol. 15, no. 24, pp. 1–26, 2025.
[70] A. Mohamed, R. R. Atta, A. A. Kotp, F. I. Abo El-Ela, H. Abd El-Raheem, A. Farghali, D. H. M. Alkhalifah, W. N. Hozzein, and R. Mahmoud, "Green synthesis and characterization of iron oxide nanoparticles for the removal of heavy metals (Cd^{2+} and Ni^{2+}) from aqueous solutions with antimicrobial investigation," *Scientific Reports*, vol. 13, no. 1, pp. 1–30, 2023.
[71] A. Singh, S. Kharbanda, F. Wan, B. Ravelo, A. Sharma, Y. Slimani, K. Yadav, P. Thakur, and A. Thakur, "Investigating morphological, optical and magnetic properties of blended novel ZnO-Ag/$NiFe_2O_4$ nanocomposite," *Inorganic Chemistry Communications*, vol. 163, p. 112357, 2024.
[72] A. S. Babar, S. A. S. Chatha, and A. U. Haq, "Innovative synthesis of Fe doped ZnO-zeolite composite for advanced applications," *Journal of the Chemical Society of Pakistan*, vol. 47, no. 5, pp. 474–486, 2025.
[73] K. Akubo, M. A. Nahil, and P. T. Williams, "Aromatic fuel oils produced from the pyrolysis-catalysis of polyethylene plastic with metal-impregnated zeolite catalysts," *Journal of the Energy Institute*, vol. 92, no. 1, pp. 195–202, 2019.
[74] M. Ulfa and I. S. Rohmah, "Thermal-induced structural evolution of mesoporous oxides Fe–Co–Ni for enhanced visible-light dye degradation," *Next Materials*, vol. 9, p. 101024, 2025.
[75] A. El Jery, M. Aldrdery, N. Ghoudi, M. Moradi, I. H. Ali, H. H. Tizkam, and S. S. Sammen, "Experimental investigation and proposal of artificial neural network models of lead and cadmium heavy metal ion removal from water using porous nanomaterials," *Sustainability*, vol. 15, no. 19, 2023.
[76] R. Nurwidiyani, D. A. Triawan, and C. D. Sigiro, "Adsorption isotherm and kinetic studies of chitosan–coffee husk carbon composite beads for the removal of Congo red and methylene blue," *ALKIMIA: Jurnal Ilmu Kimia dan Terapan*, vol. 9, no. 1, pp. 39–45, 2025.
[77] Z. Mulushewa, W. T. Dinbore, and Y. Ayele, "Removal of methylene blue from textile waste water using kaolin and zeolite-x synthesized from Ethiopian kaolin," *Environmental Analysis, Health and Toxicology*, vol. 36, no. 1, p. e2021007, 2021.
[78] S. T. Al-Asadi, F. F. Al-Qaim, H. F. S. Al-Saedi, I. F. Deyab, H. Kamyab, and S. Chelliapan, "Adsorption of methylene blue dye from aqueous solution using low-cost adsorbent: Kinetic, isotherm adsorption, and thermodynamic studies," *Environmental Monitoring and Assessment*, vol. 195, no. 6, p. 676, 2023.
[79] W. M. Saod, I. W. Oliver, A. Contini, and V. Zholobenko, "Synthesis and characterisation of an iron oxide mesoporous silica nano-composite and its application in removal of methylene blue dye," *Journal of Molecular Structure*, vol. 1319, p. 139390, 2025.
[80] M. U. Rehman, A. Manan, M. Uzair, A. S. Khan, A. Ullah, A. S. Ahmad, A. H. Wazir, I. Qaz, and M. A. Khan, "Physicochemical characterization of Pakistani clay for adsorption of methylene blue: Kinetic, isotherm and thermodynamic study," *Materials Chemistry and Physics*, vol. 269, p. 124722, 2021.

Received: 17/04/2026; Revised: 25/04/2026; Accepted: 28/04/2026; Published: 15/05/2026